JMEPEG (2018) 27:4645–4654
https://doi.org/10.1007/s11665-018-3570-9

1059-9495/$19.00

Tribological Behavior and Wear Mechanism of TZ20 Titanium Alloy After Various Treatments

S.X. Liang, L.X. Yin, L.Y. Zheng, H.L. Xie, J.X. Yao, M.Z. Ma, and R.P. Liu

(Submitted December 14, 2017; in revised form July 31, 2018; published online August 14, 2018)

Abrasion is one of the most common failure forms of metals and alloys. The study of the friction and wear behavior of metals and alloys is greatly beneficial to improve their long life and safe service. The friction coefficient, weight loss, specific wear rate, and wear mechanism of Ti-20Zr-6.5Al-4V (TZ20) alloy after various treatments were investigated using a pin–disk-type wear apparatus at various normal loads. The wear results revealed that at a normal load, the friction coefficient steadily decreased, whereas the weight loss increased. By contrast, different specimens displayed distinct variation trends of specific wear rate with respect to the normal load. Further investigations indicated that the effects of hardness and toughness on the wear properties were markedly influenced by the normal load. The main characteristic of the abrasion surface gradually changed from grooves to plastic deformation as the normal load increased. The findings promote the practical application of TiZrAlV series alloys and expand wear theory.

Keywords heat treatment, tribological behavior, TZ20 alloy, wear mechanism

1. Introduction

Wear is one of the most common failure forms of metal components, particularly active components (Ref 1). Thus, numerous studies have investigated the friction and wear of metals and alloys. The tribological properties of Ti alloys are poor because of their low resistance to plastic shearing and low work hardening effect (Ref 2, 3). However, the tribological behavior is an important property in the practical application of Ti alloys as structural materials. Thus, the practical application of new Ti alloys requires an evaluation of their friction and wear behavior.

To date, the wear resistance of Ti-based alloys can be improved using numerous methods, which can generally be divided into three groups: surface treatment (Ref 4-6), heat treatment (Ref 7, 8), and integral alloying (Ref 9-11). Although surface treatment can markedly improve the wear resistance of metals and alloys, this technique only improves the wear resistance of a surface with a finite thickness. As such, the improvement wears out after that hardened thickness was consumed. Moreover, many applications, such as bearings, require a high surface wear resistance and an integral wear resistance. Thus, the integral wear resistance of materials must be improved. Although integral alloying can improve the wear resistance of metals and alloys, this strategy is limited by excessive uncertainty in terms of the kind and amount of element, alloying method, and subsequent processing. Heat treatment can adjust and improve the integral wear resistance of metals and alloys and can be applied as the final processing for parts. Thus, the effects of heat treatment on the wear resistance of Ti alloys must be investigated and further improved.

The recently developed TiZrAlV series alloys (Ref 12-14) are characterized by favorable mechanical properties, such as low density, ultrahigh strength, and favorable plasticity. These alloys show promising application as structural materials in aerospace, navigational, and automotive fields. The friction and wear behavior of TiZrAlV series alloys have been experimentally investigated. Zhong et al. (Ref 7) investigated the friction and wear behavior of an annealed Ti-20Zr-6.5Al-4V (TZ20) alloy sliding against 440C steel in a vacuum and found that the friction coefficient of the TZ20 alloy ranged from 0.34 to 0.43. Zhong et al. (Ref 15) also investigated the influence of sliding velocity on the tribological properties of the TZ20 alloy in a vacuum. Their results revealed that with increasing sliding velocity, the friction coefficient became parabolic, whereas the wear volume increased monotonically. Zhang et al. (Ref 16) investigated the tailoring microstructure and tribological properties of a cold deformed TiZrAlV alloy and revealed that the wear resistance of the special heterogeneous lamellar-structured specimen was superior to that of equiaxed grain-structured and dual-phase lamellar-structured specimens. The friction and wear behavior of metals and alloys greatly depend on the friction conditions and properties of friction pairs (Ref 17-20). However, studies on the wear behavior of TiZrAlV series alloys have been conducted at special experimental conditions, thereby rendering these materials inadequate for practical applications. Thus, the tribological behavior of TiZrAlV series alloys must be systematically analyzed to promote its practical actual applications.

As a representative of TiZrAlV series alloys, TZ20 alloy and its tribological behavior were systematically investigated at various sliding conditions. The effects of heat treatment on their wear resistance were also analyzed. The wear mechanism of the TZ20 alloy was also assessed. These findings can promote the practical applications of the new TiZrAlV series alloys and expand the wear theory of metals and alloys.

S.X. Liang, L.X. Yin, L.Y. Zheng, H.L. Xie, and **J.X. Yao**, College of Materials Science and Engineering, Hebei University of Engineering, Handan 056038, China; and **M.Z. Ma** and **R.P. Liu**, State Key Laboratory of Metastable Materials Science and Technology, Yanshan University, Qinhuangdao 066004, China. Contact e-mails: liangshx@hebeu.edu.cn and mz550509@ysu.edu.cn.

2. Materials and Experimental Procedure

Sponge Ti (99.7 wt.%), sponge Zr (Zr + Hf ≥ 99.5 wt.%), industrially pure Al (99.5 wt.%), and V (99.9 wt.%) were used to prepare the Ti-20Zr-6.5Al-4V (wt.%, shortened as TZ20) alloy. The raw materials were blended and pressed into a rod-like electrode. The raw material rod was melted thrice in a vacuum consumable electro-arc furnace to ensure a uniform chemical composition. The ingots were subjected to combined treatments of homogenization, breakdown forging, second forging, and final forging, as shown in Ref 21. The final TZ20 alloy used in this study had the following composition (mass fraction, %): 19.2 Zr, 6.48 Al, 3.86 V, 0.771 Na, 0.707 Hf, 0.215 Fe, and balanced Ti. The onset and end of the transition temperatures of the TZ20 alloy were 789 and 946.4 °C, respectively (Ref 21). Specimens with dimensions of 70 mm (length) × 15 mm (width) × 10 mm (thickness) were cut from the forged ingots for various heat treatments as shown in Table 1. The phase composition, microstructure, hardness, and tensile properties of the specimens at various treatments were determined using an x-ray diffractor (XRD) with Cu Kα radiation, an Olympus 3D opto-digital microscope, a digital display micro-Vickers hardness tester at a load of 9.8 N, and an electronic universal testing machine at a strain rate of 0.1 s^{-1}.

The friction and wear behavior of the TZ20 alloy after various treatments were investigated using pin–disk wear pairs on a vertical universal friction wear tester. The wear tests were conducted in accordance with the "Standard Test Method for Wear Testing with a Pin-on-Disk Apparatus (ASTM G99-05(2016))" (Ref 22) at sliding conditions in the absence of lubricants. The pins were cylindrical specimens with the size of ϕ4.8 mm × 15 mm that were sectioned from various treated specimens and further smoothed by grinding using 600#, 800#, 1000#, and 1200# waterproof abrasive papers. The quenched 45# steel, which has a hardness of approximately 390 HV, was processed into standard disks with sizes ranging from ϕ 38 mm × 11 mm to ϕ54 mm × 11 mm for the friction and wear tests. The tests were performed in air by applying normal loads of 25, 50, and 100 N at sliding velocity of ~ 1.5 m/s (60 r/min) for 900 s. The testing parameters were selected based on previous investigations on Ti alloys (Ref 7, 23-26) to establish mild to severe sliding wear conditions. The wear weight loss of the pins was measured by a precision balance (0.1 mg). The surface morphology of specimens after wear was observed using an Olympus 3D opto-digital microscope.

All data were tested at least three times to avoid probabilistic results. The data points denoted in figures are the average values.

3. Results

3.1 Microstructure and Mechanical Properties of the TZ20 Alloy After Various Treatments

Figure 1 shows the XRD patterns of the TZ20 alloy after various treatments. The as-received and annealed specimens were composed of a major α phase and a small amount of β phase. By contrast, the XRD pattern of the quenched specimen differed significantly from that of the other two specimens. The phase composition of the quenched specimen includes a major retained β phase and a spot of α" martensite. The obtained XRD results were consistent with previous reports (Ref 21, 27, 28). Figure 2 shows the microstructure of the TZ20 alloy after various treatments. The micrographs in Fig. 2 indicate that both the as-received and annealed specimens had a typical basketweave microstructure, whereas the α plates in the annealed specimens were coarser than those in the as-received specimens. By contrast, the micrograph of the quenched specimen displayed no coarse α plates and numerous short acicular grains. According to the current XRD results and the literature (Ref 28), the short acicular grains were α" phase.

Table 2 lists the mechanical properties of the TZ20 alloy after different treatments. The yield strength, tensile strength, elongation, and static toughness of the as-received specimen were approximately 1286, 1426 MPa, 2.8%, and 43.2 kJ/m^2, respectively. The yield and tensile strengths of the annealed specimen were decreased to 1123 and 1248 MPa, respectively. Conversely, the plasticity of the annealed specimen in terms of elongation and static toughness was sharply increased to 9.3% and 114.5 kJ/m^2, respectively. Compared with the as-received and annealed specimens, the quenched specimen had the lowest strength and the highest plasticity and toughness. The yield strength of the quenched specimen was only 395 MPa. The decrease in the strength of the annealed specimen relative to that of as-received specimen was primarily due to the coarse α plates. The sharp decrease in the yield strength of the quenched specimen was due to the soft α" martensite. According to the literature (Ref 29-31), TiZrAlV series alloys with major retained β phase and soft α" martensite had low strength but could easily facilitate a stress-induced martensitic transition during a tensile test. The stress-induced martensitic transition requires an additional stress and yields extra strain. Thus, the quenched specimen exhibited a significantly lower yield

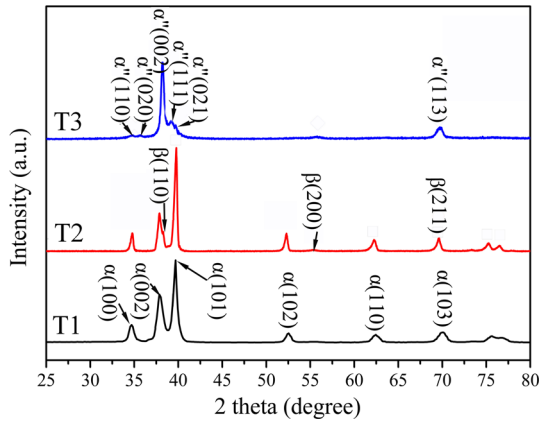

Fig. 1 XRD of TZ20 alloy after various heat treatments

Table 1 Details of heat treatments performed on the TZ20 alloy

Specimen	Treatment	Details
T1	As-received	Melting, homogenization, breakdown, forging
T2	Annealing	900 °C, 30 min, cooling in furnace to 500 °C then in the air
T3	Solution treatment	900 °C, 30 min, water quenching within 5 s

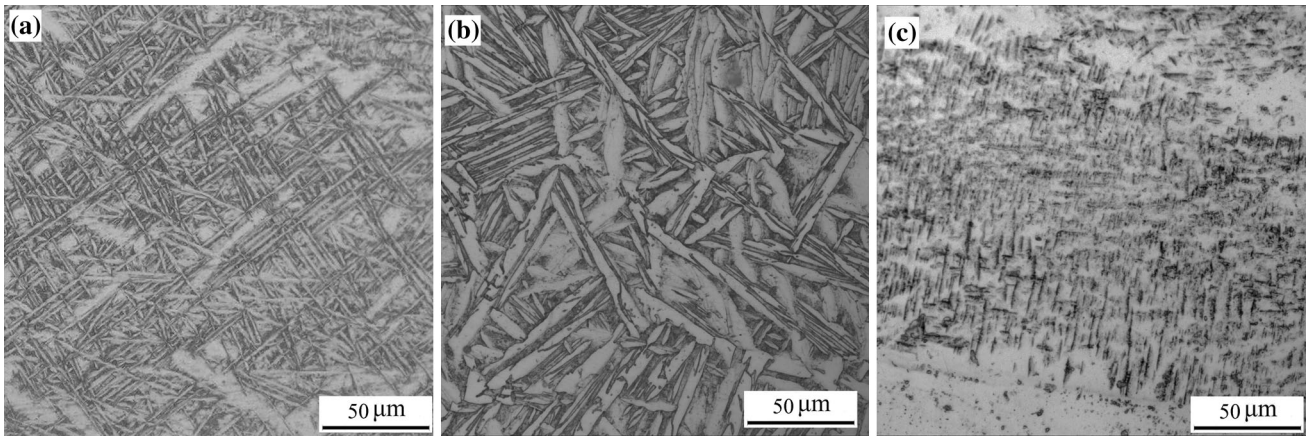

Fig. 2 Microstructure of TZ20 alloy after various treatments (a) as-received, (b) annealed, and (c) solution treatment

Table 2 Mechanical properties of the TZ20 alloy after various treatments

Specimen	$\sigma_{0.2}$, MPa	σ_b, MPa	ε, %	U_T, kJ/m^2	Hv1
T1	1286	1426	2.8	43.2	375
T2	1123	1248	9.3	114.5	361
T3	395	1161	13.8	122.9	328

U_T: static toughness, total areas under the stress–strain curve

strength, a comparable tensile strength, and high elongation and toughness. Table 2 also presents the hardness results of the examined alloy atwent various treatments. The trend of hardness was consistent with that of tensile strength.

3.2 Tribological Behavior of TZ20 Alloy Under Different Conditions

The friction coefficient (*FC*) versus test time curves of the TZ20 alloy at different conditions were investigated, and results are depicted in Fig. 3. As shown in Fig. 3(a), the friction coefficient remained in a stable range when the test duration reached 4500 s. Thus, the duration of the other tests was set to 900 s. The average *FC* of TZ20 at various conditions was obtained based on the *FC* versus time curves. The tribological properties of the TZ20 alloy at different conditions were determined by combining the *FC* and weight loss results, and the results are provided in Fig. 4. Figure 4(a) shows the variation of the *FC* of the TZ20 alloy after various treatments with respect to the normal load. As the normal load increased from 25 to 100 N, the *FC* of the as-received specimen was gradually decreased from 0.38 to 0.32, and that of the annealed specimen stabilized at around 0.35. This *FC* range was similar to that of Ti alloys in previous reports (Ref 15, 20, 32). The *FC* of the quenched specimen was markedly decreased from 0.42 to 0.21 as the normal load was increased from 25 to 50 N, and it stabilized around that range as the normal load was further increased. Figure 4(b) shows the variations of the weight loss of the TZ20 alloy that atwent various treatments at a normal load. The weight loss of all specimens after various treatments increased with increasing normal load. Similar results have been reported in the literature (Ref 33, 34). Although the variations of the weight losses of all examined specimens at normal load were similar, the values of the weight loss of the different specimens vastly differed. The as-received specimen had the maximum weight loss, which was almost double that of the quenched specimen. The specific wear rate *Ws*, which is defined by the volume loss of materials at the action of per unit applied load and per unit distance, was also investigated. Figure 4(c) shows the variation of the *W*s of various specimens with respect to the normal load. The variation of the *Ws* of the as-received specimen at normal load was parabolic. The maximum value was approximately 2.0×10^{-4} mm^3/(Nm) at a normal load of 50 N. The *Ws* of the annealed specimen was gradually increased approximately 0.4×10^{-4} to 0.8×10^{-4} mm^3/(Nm) as the normal load was increased from 25 to 100 N. By contrast, the trend of the *Ws* versus normal load curve for the quenched specimen was inverse parabolic. The *Ws* was approximately 0.6×10^{-4} mm^3/(Nm) at the normal loads of 25 and 100 N and 0.38×10^{-4} mm^3/(Nm) at 50 N.

3.3 Correlation Between Hardness and Wear Properties

Figure 5 presents the correlations between the wear properties of the TZ20 alloy and hardness at different normal loads. At a normal load of 25 N, the variations of weight loss, *FC,* and *Ws* with respect to hardness were similar. That is, the wear properties initially decreased and subsequently increased as the hardness increased. The minimum values were detected at the hardness of 361 HV. Comparison of Fig. 5(b) and (a) implied that the relationships between the wear properties and hardness at the normal load of 50 N obviously differed from those at 25 N. Weight loss, *FC*, and *Ws* increased with increasing hardness at the normal load of 50 N. As the normal load was further increased to 100 N, the relationships between the wear properties and hardness continued to change. The trend of the *Ws* versus hardness curve at a normal load of 100 N was similar

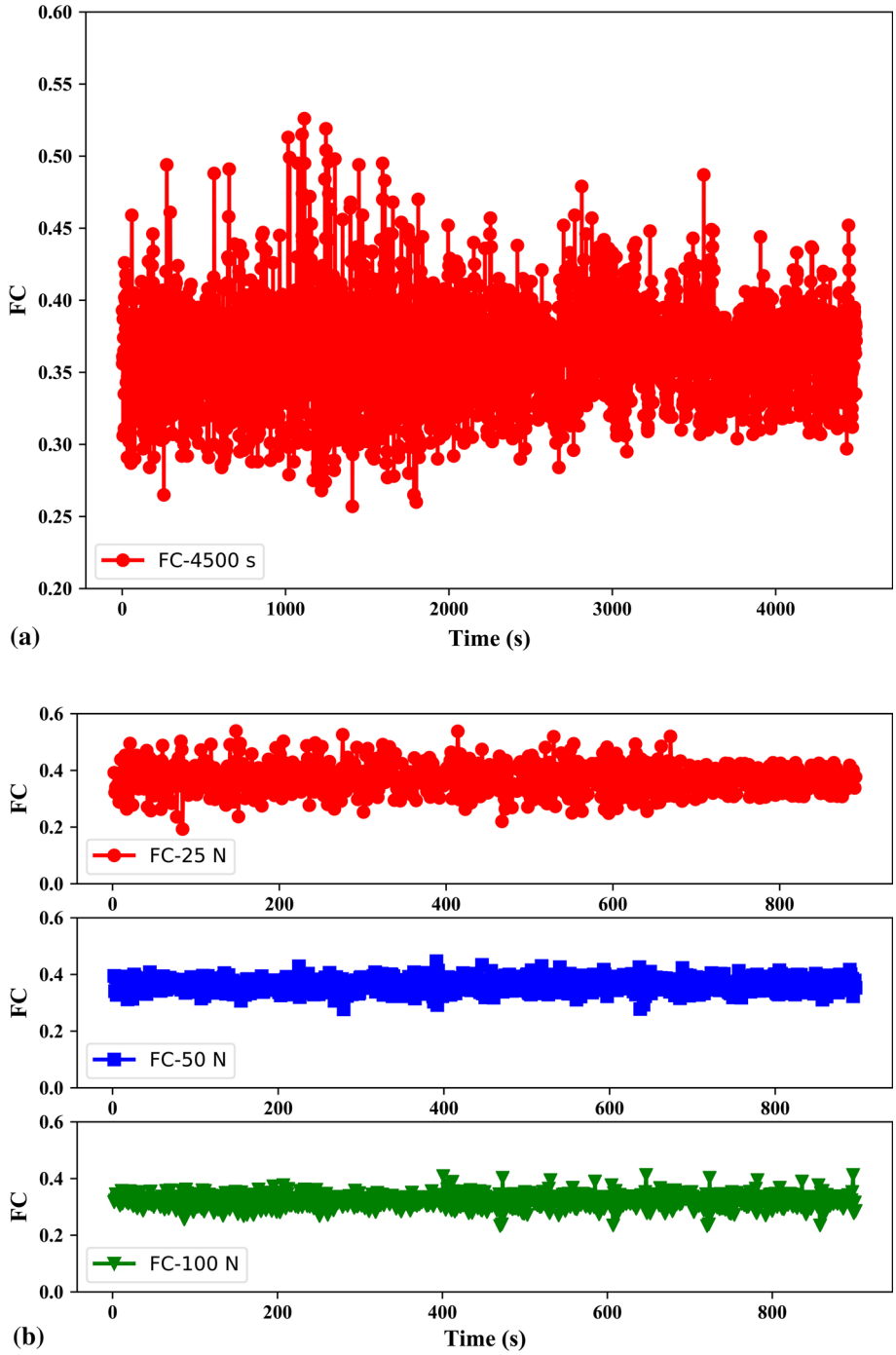

Fig. 3 Friction coefficient vs. time duration of (a) 4500 s at 25 N of the as-received specimen, and 900 s at various normal loads of (b) as-received, (c) annealed, and (d) solution treated specimens

to that at 50 N. Weight loss and *FC* initially increased and subsequently. In other words, hardness greatly affected the wear properties. However, the trend of the wear properties versus hardness curve was markedly changed by the normal load.

3.4 Correlation Between Toughness and Wear Properties

The relationships between the wear properties and static toughness were also investigated, and the results are provided in Fig. 6. At a normal load of 25 N, weight loss, *FC,* and *Ws* displayed similar variations with respect to static toughness. That is, the wear properties initially decreased and subsequently increased as the static toughness increased. However, as shown in Fig. 6(b), weight loss, *FC,* and *Ws* decreased gradually with increasing static toughness at a normal load of 50 N. Comparison of Fig. 6(c) and (b) indicated that the variations of *FC* and *Ws* with respect to static toughness at a normal load of 100 N were similar to that at 50 N. The variation of weight loss with respect to static toughness was markedly changed. The weight loss was substantially increased from approximately 27 to 50 mg as the static toughness increased from 43 to 115 kJ/m^2 and then decreased to nearly 40 mg as the static toughness was

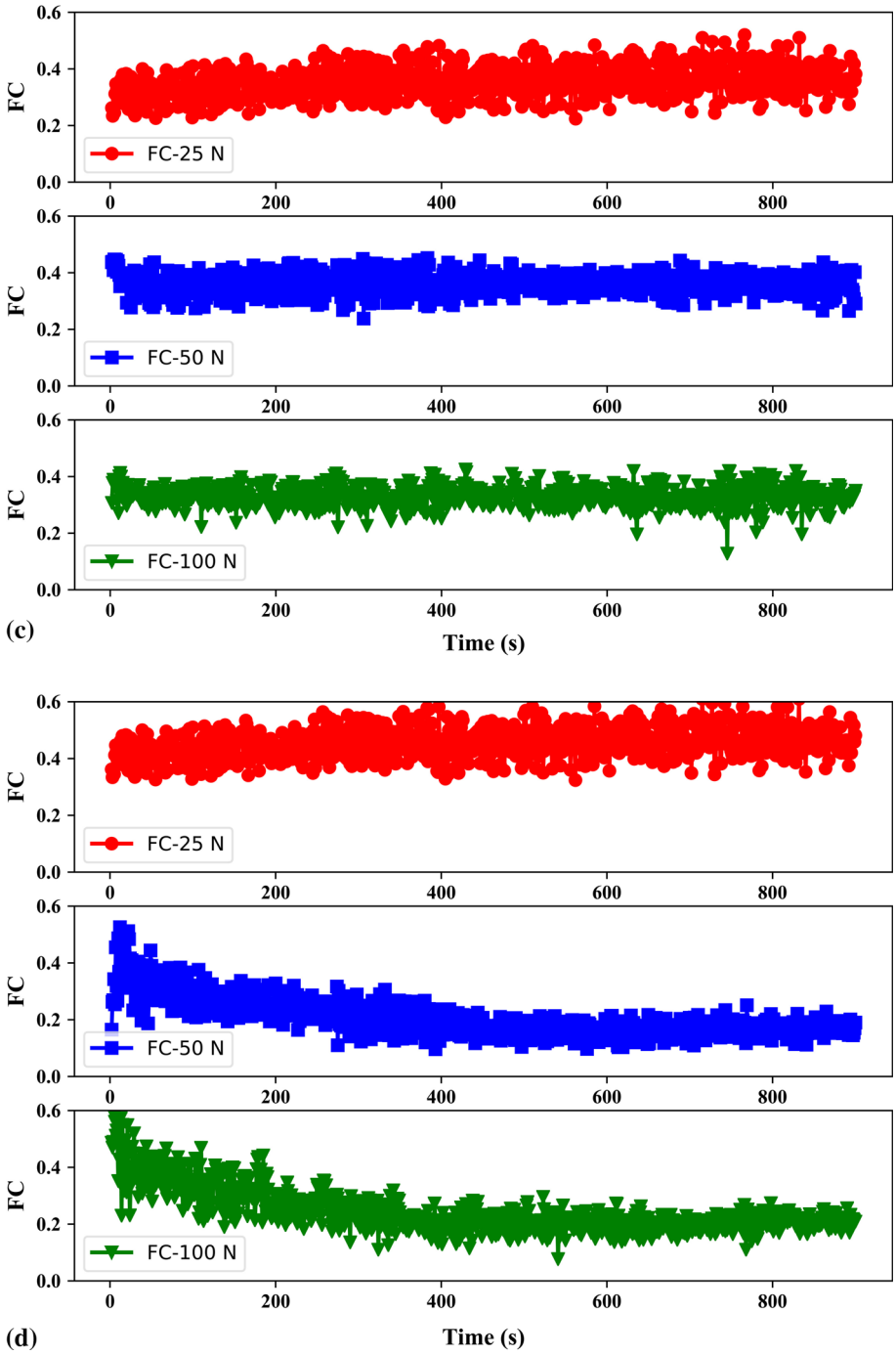

Fig. 3 continued

further increased to 123 kJ/m^2. In addition, the literature (Ref 35-37) also showed that the toughness strongly influenced the wear properties of Ti alloys.

3.5 Wear Surface and Mechanism

These results suggest that the normal load of the friction test can obviously affect the tribological behavior of TZ20 alloys after various treatments. To investigate the wear mechanism at various normal loads, the worn surface of the as-received specimen was observed and analyzed. The worn surface graphs of the as-received specimen are presented in Fig. 7. The worn track of the specimen at a normal load of 25 N in Fig. 7(a) indicates that this track was mainly characterized by grooves and some debris. These debris were formed during friction and acted as abrasive particles that promoted abrasion. Thus, the main wear form of the specimen tested at a normal load of 25 N was abrasive wear. The 3D depth and 2D profile graphs indicate that the average depth of the grooves after testing at 25 N was approximately 6.3 μm, suggesting that the wear at this condition was relatively weak. Figure 7(b) shows the worn

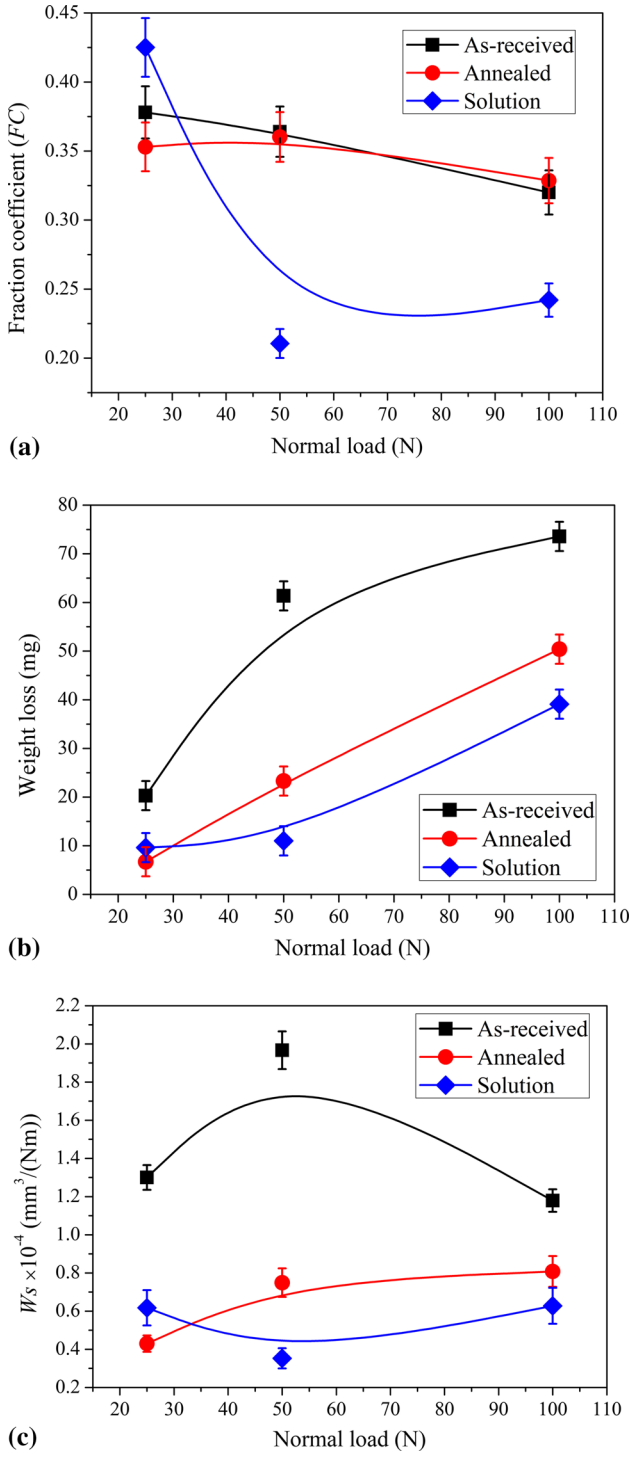

Fig. 4 Wear properties of specimens at various normal loads (a) friction coefficient, (b) weight loss, and (c) specific wear rate

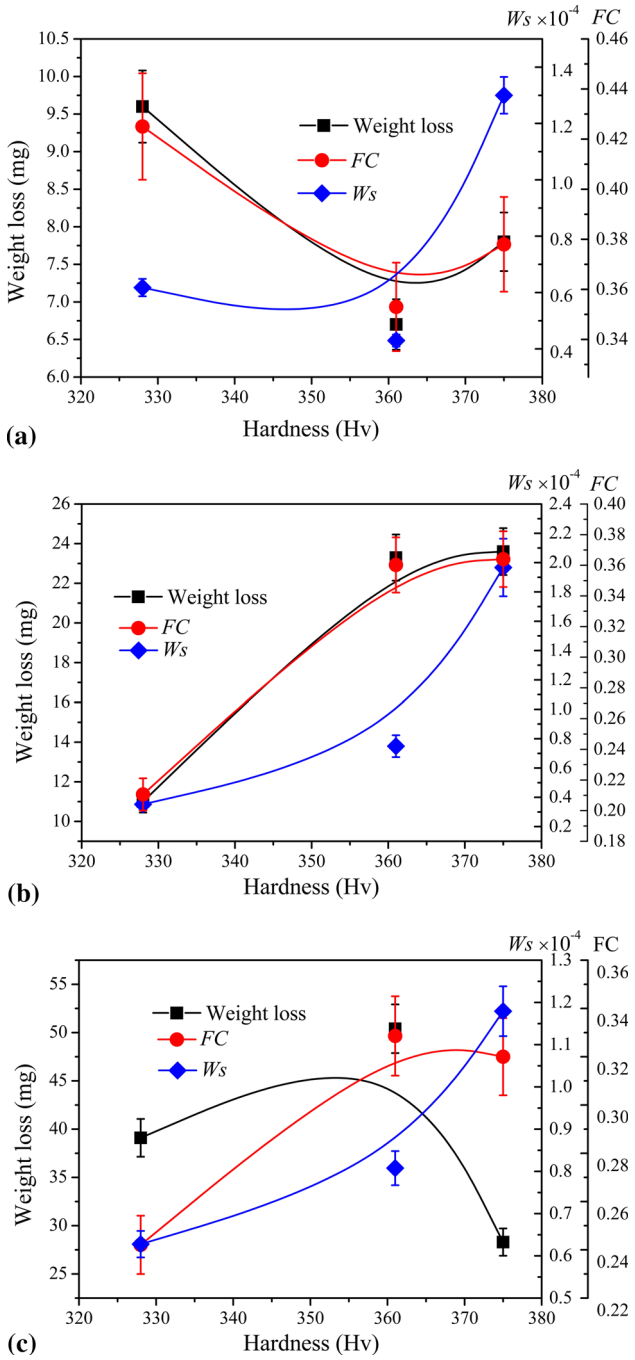

Fig. 5 Variations of wear properties of TZ20 alloy with hardness at a normal load of (a) 25 N, (b) 50 N, and (c) 100 N

track at a normal load of 50 N, which was also mainly characterized by obvious grooves. Wave-like patterns were also observed on the wear surface. According to the literature (Ref 15, 38), these wave-like patterns resulted from the plastic deformation during friction at a high normal load. Given that the shear stress component of the normal load was greater than the shear strength of the friction materials, shear deformation would occur, and wave-like patterns would be formed (Ref 39, 40) As shown by the 3D depth and 2D profile graphs in Fig. 7(e), the depth and width of the grooves on the wear surface after testing at 50 N were significantly higher than that at 25 N. The average depth of the grooves after testing at 50 N was approximately 13.5 μm. Thus, the abrasion at 50 N was more severe than that at 25 N, and the main wear form of the specimen tested at 50 N was the mixed form of abrasive and adhesive wear. As the normal load was further increased to 100 N, the worn track (Fig. 7c) became obviously different from that at the other two normal loads. The obvious characteristic of the wear surface at 100 N was the wave-like pattern. Grooves could still be observed, but they were no longer the major feature. Furthermore, numerous bent bound-

aries of the grooves were observed after testing at 100 N. Bent boundaries are typical stacks of severe surface plastic deformation (Ref 41). The 3D depth graph shows that the average depth of the grooves after testing at 100 N was approximately 10.4 μm. The shallow and wide grooves further proved that a severe plastic deformation occurred and yielded stack. Thus, the main wear form of the specimen tested at a normal load of 100 N was adhesive wear.

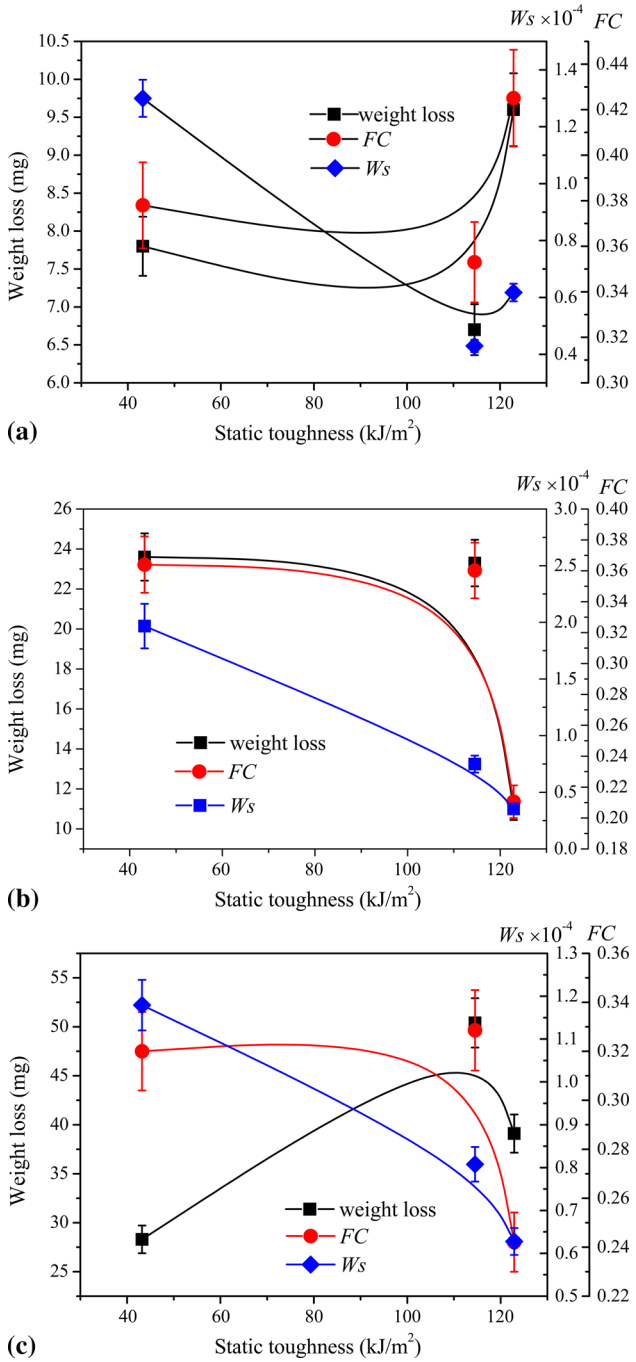

Fig. 6 Variations of wear properties of TZ20 alloy with static toughness at a normal load of (a) 25 N, (b) 50 N, and (c) 100 N

4. Discussion

The tribological behavior of metals and alloys is related the friction conditions (such as normal load, friction velocity, and temperature) and the material properties (such as hardness, toughness, and strength). Correlations between the wear properties of the TZ20 alloy and the normal load showed that with increasing normal load, the friction coefficient decreased, whereas the weight loss and the specific wear rate increased. The variations of the wear properties with respect to the normal load exhibited the general rule for most of metals and alloys. The main reason is that most particles lost their cutting edges and particles damaged during the abrasive process, and such loss would worsen with increasing load (Ref 42, 43).

The relationships between the hardness and the wear properties demonstrated that the friction coefficient and weight loss of the TZ20 alloy decreased with increasing hardness at a low normal load of 25 N. This trend is the typical result reported in the literature (Ref 44). The main reason is that improving the hardness can obstruct the break of the surface bulges (Ref 1). However, reverse trends were detected at high normal loads of 50 and 100 N. The relationships between the toughness and wear properties of the specimens tested at high normal loads of 50 and 100 N also exhibited reverse trends to that at 25 N. That is, *FC* and weight loss increased with increasing static toughness at low normal load of 25 N, but they decreased with increasing static toughness at high normal loads of 50 and 100 N. The obvious effects of the normal load on the variations of the wear properties with respect to hardness and toughness were due to two main reasons. The first is the different wear forms at various normal loads. The main wear form tested at 25 N was abrasive wear, whereas tracks of plastic deformation were observed on the worn surface as the normal load was increased to 50 N. As the normal load was further increased to 100 N, the plastic deformation became the major wear character. Plastic deformation on the surface during friction can drastically affect the wear properties of materials with high hardness and toughness (Ref 45, 46). Thus, the variations of the wear properties with respect to both hardness and toughness significantly changed with increasing normal load. The second reason is the martensitic transition. The XRD result in Fig. 1 states that the α" martensite was the major phase of the quenched specimen. According to the literature (Ref 47, 48), a stress-induced martensitic transition can easily occur in Ti alloys composed of α" martensite and β phase during plastic deformation. The stress-induced martensitic transition in TiZrAlV series alloys can improve the strength and the hardness (Ref 28, 31). That is, the plastic deformation on the surface of the quenched specimen during friction can induce a martensitic transition and change the wear resistance (Ref 49). Thus, the variations of the wear properties with respect to hardness and toughness at high normal loads over 50 N were significantly different from that at a low load. Ehtemam-Haghighi et al. (Ref 10) found a similar result that the wear rate of the Ti-*x*Nb-7Fe alloy with highest α" martensite concentration had the lowest wear rate.

The results of this study demonstrated that the wear properties of TZ20 alloys greatly depend on heat treatment processing. The variation degrees of the wear properties after various heat treatments were not significant. The *FC* of the TZ20 alloy ranged from 0.35 to 0.42. The weight loss varied from 6.7 mg to 9.6 mg. W_s ranged from 4.3×10^{-5} to

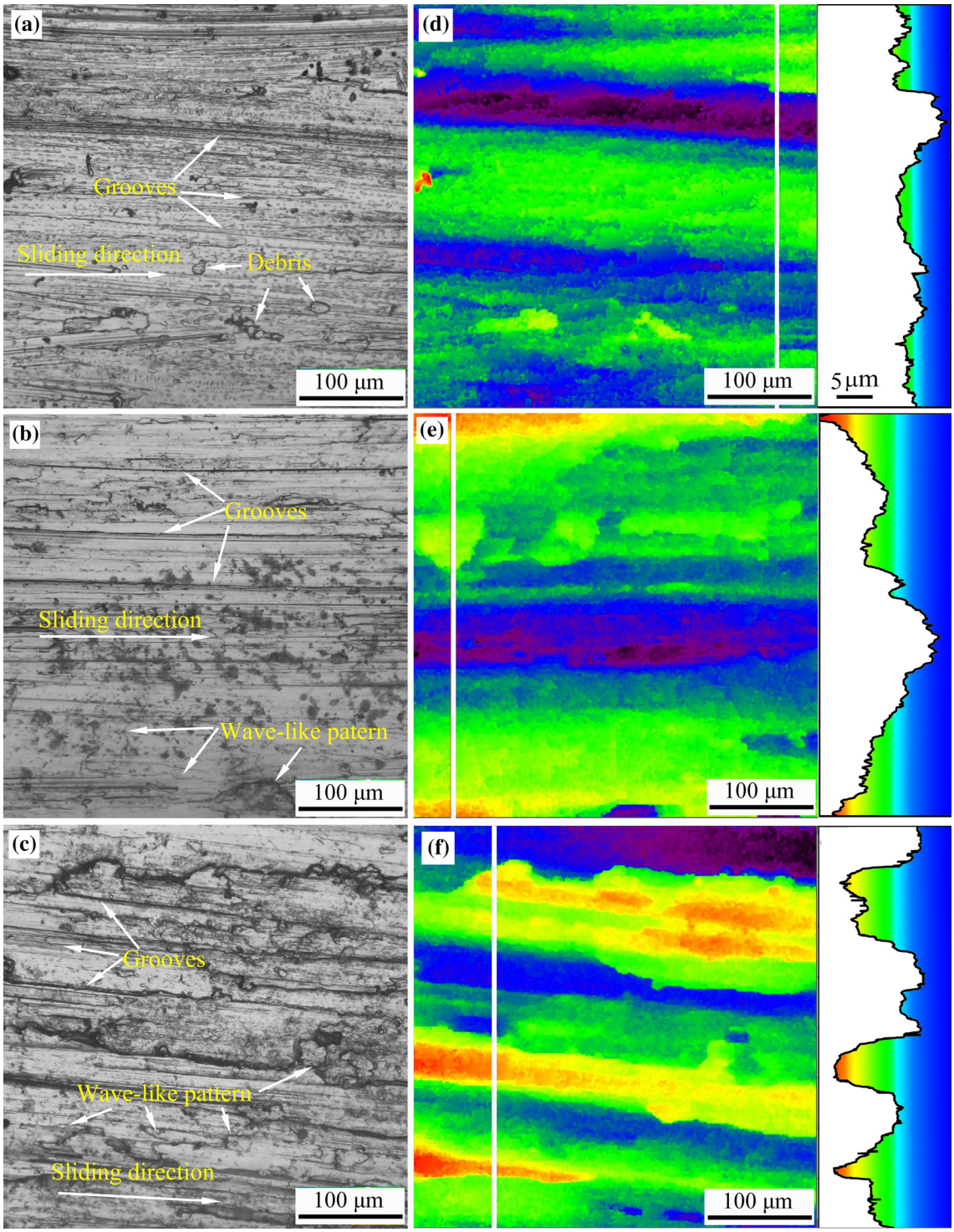

Fig. 7 Worn trace of the as-received specimen at normal load of (a) 25 N, (b) 50 N, (c) 100 N, and corresponding 3D depth and 2D profile graphs (d) to (f)

1.3×10^{-4} $mm^3/(Nm)$. The wear properties of the Ti alloys can be markedly changed after surface treatment and/or integral alloying treatment. Chen et al. (Ref 6) showed that the wear resistance of the 5% CeO_2 coating on the Ti6Al4V was enhanced by 24.59-fold of that of the substrate. Ehtemam-Haghighi et al. (Ref 10) demonstrated that the wear rate of the Ti-*x*Nb-7Fe alloy was gradually increased from 3×10^{-15} to 1×10^{-13} m^3/m as the Nb content was increased from 0 to 11%. The notable difference in the effects of these methods on the wear resistance resulted from their effect on hardness. Therefore, on the basis of the current results and those reported in the literature, the wear resistance of metals and alloys strongly depends on their hardness (Ref 6, 50) and/or the ratio of the hardness to the elastic modulus (Ref 9, 10).

5. Conclusions

The tribological behavior and wear mechanism of the TZ20 alloy as a representative of TiZrAlV series alloys were investigated in this work. Overall, the friction coefficient of the TZ20 alloy after various treatments decreased, whereas the weight loss increased with increasing normal load. However, the specific wear rate of various specimens exhibited different trend variations with the normal load. Hardness and toughness also markedly affected the wear properties of the TZ20 alloy. However, the variations of the wear properties with respect to hardness and toughness were greatly affected by the normal load. Abrasive wear was the main wear form of the TZ20 alloy at a low normal load of 25 N. As the normal load was increased to over 50 N, plastic deformation occurred on the wear surface and worsened with increasing normal load. Consequently, the main wear form was gradually shifted to adhesive wear.

Acknowledgments

This work was supported by The Youth Talent Support Program of Hebei Province of China, The Excellent Going Abroad Experts' Traning Program in Hebei Province, The Natural Science Foundation of Hebei Provincial Department of Education (Grant No. A2016002024), The National Natural Science Foundation of China (Grant Nos. 51531005/51571174), The Natural Science Foundation of Hebei Province of China (Grant No. E2015402111) and The Open Foundation of State Key Laboratory of Metastable Materials Science and Technology (Grant No. 201606).

References

1. P.L. Menezes, S.P. Ingole, M. Nosonovsky et al., *Tribology for Scientists and Engineers*, Springer, New York, 2013
2. P. Jiang, X.L. He, X.X. Li et al., Wear Resistance of a Laser Surface Alloyed Ti-6Al-4V Alloy, *Surf. Coat. Technol.*, 2000, **130**(1), p 24–28
3. A. Molinari, G. Straffelini, B. Tesi et al., Dry Sliding Wear Mechanisms of the Ti6Al4V Alloy, *Wear*, 1997, **208**(1), p 105–112
4. C. Prakash, H.K. Kansal, B.S. Pabla et al., Potential of Silicon Powder-Mixed Electro Spark Alloying for Surface Modification of β-Phase Titanium Alloy for Orthopedic Applications, *Mater. Today Proc.*, 2017, **4**(9), p 10080–10083
5. F. Movassagh-Alanagh, A. Abdollah-Zadeh, M. Aliofkhazraei et al., Improving the Wear and Corrosion Resistance of Ti-6Al-4V Alloy by Deposition of TiSiN Nanocomposite Coating with Pulsed-DC PACVD, *Wear*, 2017, **390**, p 93–103
6. T. Chen, D. Liu, F. Wu et al., Effect of CeO2 on Microstructure and Wear Resistance of TiC Bioinert Coatings on Ti6Al4V Alloy by Laser Cladding, *Materials*, 2017, **11**(1), p 58
7. H. Zhong, L.Y. Dai, Y. Yue et al., Friction and Wear Behavior of Annealed Ti-20Zr-6.5 Al-4V Alloy Sliding Against 440C Steel in Vacuum, *Tribol. Int.*, 2017, **109**, p 571–577
8. S. Heilig, M. Ramezani, T. Neitzert, et al., Investigation of Friction and Wear Properties of Duplex-Annealed Ti-6Al-2Sn-4Zr-2Mo Against Hardened AISI E52100 at Linear Reciprocating Motion. *Trans. Indian Inst. Met.*, 2018, **71**(5), p 1257–1264
9. S. Ehtemam-Haghighi, G. Cao, and L.C. Zhang, Nanoindentation Study of Mechanical Properties of Ti Based Alloys with Fe and Ta Additions, *J. Alloys Compd.*, 2017, **692**, p 892–897
10. S. Ehtemam-Haghighi, K.G. Prashanth, H. Attar et al., Evaluation of Mechanical and Wear Properties of TixNb7Fe Alloys Designed for Biomedical Applications, *Mater. Des.*, 2016, **111**, p 592–599
11. H. Choi, S. Shil'ko, J. Gubicza et al., Study of the Compression and Wear-Resistance Properties of Freeze-Cast Ti and Ti-5W Alloy Foams for Biomedical Applications, *J. Mech. Behav. Biomed. Mater.*, 2017, **72**, p 66–73
12. S.X. Liang, L.X. Yin, M.Z. Ma et al., A Multi-component Zr Alloy with Comparable Strength and Higher Plasticity than Zr-Based Bulk Metallic Glasses, *Mater. Sci. Eng. A*, 2013, **561**, p 13–16
13. R. Jing, S.X. Liang, C.Y. Liu et al., Aging Effects on the Microstructures and Mechanical Properties of the Ti-20Zr-6.5 Al-4V Alloy, *Mater. Sci. Eng. A*, 2013, **559**, p 474–479
14. S.X. Liang, M.Z. Ma, R. Jing et al., Preparation of the ZrTiAlV Alloy with Ultra-High Strength and Good Ductility, *Mater. Sci. Eng. A*, 2012, **539**, p 42–47
15. H. Zhong, L.Y. Dai, Y.J. Yang et al., Vacuum Tribological Properties of Ti-20Zr-6.5 Al-4V Alloy as Influenced by Sliding Velocities, *Metall. Mater. Trans. A*, 2017, **48**(11), p 5678–5687
16. G.S. Zhang, D.F. Guo, M. Li et al., Tailoring Microstructure and Tribological Properties of Cold Deformed TiZrAlV Alloy by Thermal Treatment, *Acta Metall. Sin. (English Lett.)*, 2017, **30**(5), p 493–498
17. A. Molinari, G. Straffelini, B. Tesi et al., Dry Sliding Wear Mechanisms of the Ti6Al4V Alloy, *Wear*, 1997, **208**(1), p 105–112
18. H. Choi, S. Shil'ko, J. Gubicza et al., Study of the Compression and Wear-Resistance Properties of Freeze-Cast Ti and Ti-5W Alloy Foams for Biomedical Applications, *J. Mech. Behav. Biomed. Mater.*, 2017, **72**, p 66–73
19. K. Farokhzadeh and A. Edrisy, Transition Between Mild and Severe Wear in Titanium Alloys, *Tribol. Int.*, 2016, **94**, p 98–111
20. J. Song, T. Liu, H. Shi et al., Time-Frequency Analysis of the Tribological Behaviors of Ti6Al4V Alloy Under a Dry Sliding Condition, *J. Alloys Compd.*, 2017, **724**, p 752–762
21. R. Jing, S.X. Liang, C.Y. Liu et al., Effect of the Annealing Temperature on the Microstructural Evolution and Mechanical Properties of TiZrAlV Alloy, *Mater. Des.*, 2013, **52**, p 981–986
22. ASTM G99-05, *Standard Test Method for Wear Testing with a Pin-on-Disk Apparatus*, ASTM International, West Conshohocken, PA, 2016, www.astm.org
23. R.K. Gunda and S.K.R. Narala, Tribological Studies to Analyze the Effect of Solid Lubricant Particle Size on Friction and Wear Behaviour of Ti-6Al-4V Alloy, *Surf. Coat. Technol.*, 2016, **308**, p 203–212
24. A. Amanov and S. Sasaki, A Study on the Tribological Characteristics of Duplex-Treated Ti-6Al-4V Alloy Under Oil-Lubricated Sliding Conditions, *Tribol. Int.*, 2013, **64**, p 155–163
25. X.Y. Ai, H.L. Lin, B. Zhang, et al., Hydrogen-Free Nitriding of ZrTiAlV by Double Glow Plasma Discharge Improving the Wear Resistance. *Mater. Sci. Technol.*, 2018, **34**(11), p 1–6
26. Y. Yang, C. Zhang, Y. Wang et al., Friction and Wear Performance of Titanium Alloy Against Tungsten Carbide Lubricated with Phosphate Ester, *Tribol. Int.*, 2016, **95**, p 27–34
27. S.X. Liang, L.X. Yin, L.Y. Zheng et al., The Microstructural Evolution and Grain Growth Kinetics of TZ20 Alloy During Isothermal Annealing, *Mater. Des.*, 2016, **99**, p 396–402
28. L.X. Yin, S.X. Liang, L.Y. Zheng et al., Inhibition of Martensitic Formation and Mechanical Properties of the TZ20 Alloy During Hot Rolling, *J. Alloys Compd.*, 2015, **649**, p 726–730
29. S. Neelakantan, E.I. Galindo-Nava, M.D. San et al., Modelling and Design of Stress-Induced Martensite Formation in Metastable β Ti Alloys, *Mater. Sci. Eng. A*, 2014, **590**, p 140–146
30. S. Hanada, N. Masahashi, and T.K. Jung, Effect of Stress-Induced α" Martensite on Young's Modulus of β Ti-33.6 Nb-4Sn Alloy, *Mater. Sci. Eng. A*, 2013, **588**, p 403–410
31. S.X. Liang, L.X. Yin, L.Y. Zheng et al., The Strain-Hardening Behavior of TZAV-30 Alloy After Various Heat Treatments, *J. Mater. Eng. Perform.*, 2016, **25**(2), p 530–535
32. Q. Niu, X. Zheng, M. Chen et al., Study on the Tribological Properties of Titanium Alloys Sliding Against WC-Co During the Dry Friction, *Ind. Lubr. Tribol.*, 2014, **66**(2), p 202–208
33. I. Saravanan, A.E. Perumal, R.F. Issac et al., Optimization of Wear Parameters and Their Relative Effects on TiN Coated Surface Against Ti6Al4V Alloy, *Mater. Des.*, 2016, **92**, p 23–35
34. M.R. Roy, N. Ramanaiah, and B.S.K.S.S. Rao, Sliding Wear Behavior of Ti6Al4V Implant Alloy in the Simulated Body Environment, *Int. J. Mechatron. Manuf. Autom. Eng.*, 2017, **1**(1), p 5–11
35. H. Chadda, B.K. Satapathy, A. Patnaik et al., Mechanistic Interpretations of Fracture Toughness and Correlations to Wear Behavior of Hydroxyapatite and Silica/Hydroxyapatite Filled bis-GMA/TEGDMA Micro/Hybrid Dental Restorative Composites, *Compos. B Eng.*, 2017, **130**, p 132–146

36. M. Filipovic, Z. Kamberovic, M. Korac et al., Correlation of Microstructure with the Wear Resistance and Fracture Toughness of White Cast Iron Alloys, *Met. Mater. Int.*, 2013, **19**(3), p 473–481
37. W. Cui, G. Qin, J. Duan et al., A Graded Nano-TiN Coating on Biomedical Ti Alloy: Low Friction Coefficient, Good Bonding and Biocompatibility, *Mater. Sci. Eng. C*, 2017, **71**, p 520–528
38. H. Wu, I. Baker, Y. Liu et al., Tribological Studies of a Zr-Based Bulk Metallic Glass, *Intermetallics*, 2013, **35**, p 25–32
39. H. Czichos, *Tribology: A Systems Approach to the Science and Technology of Friction, Lubrication, and Wear*, Elsevier, Amsterdam, 1978
40. F. Bin and Z.J. Luo, Finite Element Simulation of the Friction Mechanism in Plastic-Working Technology, *Wear*, 1988, **121**(1), p 41–51
41. K. Gu, J. Wang, and Y. Zhou, Effect of Cryogenic Treatment on Wear Resistance of Ti-6Al-4V Alloy for Biomedical Applications, *J. Mech. Behav. Biomed. Mater.*, 2014, **30**, p 131–139
42. A. Jourani, B. Hagège, S. Bouvier et al., Influence of Abrasive Grain Geometry on Friction Coefficient and Wear Rate in Belt Finishing, *Tribol. Int.*, 2013, **59**, p 30–37
43. A. Khellouki, J. Rech, and H. Zahouani, Energetic Analysis of Cutting Mechanisms in Belt Finishing of Hard Materials, *Proc. Inst. Mech. Eng. Part B J. Eng. Manuf.*, 2013, **227**(9), p 1409–1413
44. C. Trevisiol, A. Jourani, and S. Bouvier, Effect of Hardness, Microstructure, Normal Load and Abrasive Size on Friction and on Wear Behaviour of 35NCD16 Steel, *Wear*, 2017, **388–389**, p 101–111
45. A. Jourani, Effect of Roughness Geometries in Contact Mechanics, *Int. J. Mater. Prod. Technol.*, 2015, **51**(2), p 127–138
46. A. Jourani, New 3D Numerical Model of Rough Contact: Influence of Mode of Surface Deformation on Real Area of Contact and Pressure Distribution, *J. Tribol.*, 2015, **137**(1), p 011401
47. C.H. Wang, C.D. Yang, M. Liu et al., Martensitic Microstructures and Mechanical Properties of as-Quenched Metastable β-type Ti-Mo Alloys, *J. Mater. Sci.*, 2016, **51**(14), p 6886–6896
48. S. Cai, J.E. Schaffer, and Y. Ren, Stress-Induced Phase Transformation and Room Temperature Aging in Ti-Nb-Fe Alloys, *Mater. Sci. Eng. A*, 2017, **680**, p 13–20
49. M. Mehdi, K. Farokhzadeh, and A. Edrisy, Dry Sliding Wear Behavior of Superelastic Ti-10V-2Fe-3Al β-Titanium Alloy, *Wear*, 2016, **350**, p 10–20
50. W. Pawlak, K.J. Kubiak, B.G. Wendler et al., Wear Resistant Multilayer Nanocomposite WC_{1-x}/C Coating on Ti-6Al-4V titanium Alloy, *Tribol. Int.*, 2015, **82**(1), p 400–406